Grain Boundary Accumulation of Geometrically Necessary Dislocations and Asymmetric Deformations in Compatible Bicrystals with Tilted Angle Grain Boundary under Tensile Loading*

Ryouji KONDOU** and Tetsuya OHASHI***

Slip deformation in compatible bicrystal models with a tilted angle grain boundary subjected to tensile load is investigated using a finite element crystal plasticity analysis code. The accumulation of geometrically necessary dislocations (GNDs) and statistically stored dislocations (SSDs) is studied in detail. Uniform deformation was expected to occur because the mutual constraint of crystal grains through the grain boundary plane does not occur in compatible bicrystals, but some results of the analysis show asymmetric deformation with the accumulation of GNDs near the grain boundary caused by the difference in strain hardening of slip systems, kink bands perpendicular to the primary slip direction and secondary slip bands parallel to the primary slip plane with accumulation of GNDs on the primary slip system in the form of bands. The mechanism of dislocation pattern formation in the bicrystals with a tilted angle grain boundary is discussed from the viewpoint of an imaginary disclination deformation field with pair body interaction.

Key Words: Plasticity, Dislocation, Finite Element Method, Compatible Bicrystals, Tilted Angle Grain Boundary, Disclination, Kink Band, Secondary Slip Band

1. Introduction

The plastic deformation of polycrystalline metal is caused by a combination of the slip deformation and elastic deformation of each crystal grain. Since the restraint interaction of deformation occurs through the grain boundary plane by elastic incompatibility stress and strain incompatibility[1], the plastic shear deformation and accumulation of geometrically necessary dislocations[2] occur near the grain boundary. Accordingly, it is considered that the accumulation of geometrically necessary (GN) dislocations with nonuniform deformation is caused by the restraint interaction of deformation through the grain boundary plane. However, under some conditions, nonuniform deformation with a GN dislocation structure occurs in the crystal grain, even if bicrystal models satisfy the requirement[3),(4)] in which the mutual constraint of crystal grains through the grain boundary plane does not occur[5),(6)].

In our previous study, we concluded that the accumulation of GN dislocations is caused by the incompatibility of shape change[5),(6)], and that the GN dislocation structure that grows inside the crystal grain expands nonuniformly to form macroscopic deformation[6]. In this way, the investigation of bicrystal models is effective for understanding the pair interaction of crystal grains and the effect of crystal grain boundary in which the mutual constraint of crystal grains occur through the grain boundary plane.

In the case of bicrystal models with a tilted angle grain boundary, the spatial disposition of slip systems is asymmetric. The accumulation of an asymmetric GN dislocation structure with nonuniform deformation affects the restraint interaction of slip deformation in bicrystal models. In this study, the effects of asymmetric nonuniform deformation with GN dislocation structure formation on subsequent deformation in compatible bicrystal models with a tilted angle grain boundary subjected to tensile load

* Received 28th June, 2006 (No. 05-0636). Japanese Original: Trans. Jpn. Soc. Mech. Eng., Vol.72, No.713, A (2006), pp.16–23 (Received 13th June, 2005)

** Faculty of Engineering, University of the Ryukyus, 1 Senbaru, Nishihara-cho, Nakagami-gun, Okinawa 903–0213, Japan

*** Kitami Institute of Technology, 165 Koen-cho, Kitami-shi, Hokkaido 090–8507, Japan

is investigated in detail.

2. Basic Equation

Slip deformation in face-centered-cubic crystals is assumed to occur on the {111} crystal plane and in the < 110 > crystal direction. The combinations of these slip planes and slip direction defines 12 slip systems. The activation condition of slip system n is given by the Schmid law:

$$P_{ij}^{(n)}\sigma_{ij}=\theta^{(n)}, \quad P_{ij}^{(n)}\dot{\sigma}_{ij}=\dot{\theta}^{(n)}, \quad (n=1,2,\cdots,12), \tag{1}$$

and

$$P_{ij}^{(n)}=\frac{1}{2}\left\{v_i^{(n)}b_j^{(n)}+v_j^{(n)}b_i^{(n)}\right\}, \tag{2}$$

where σ_{ij} and $\theta^{(n)}$ denote the stress and the critical resolved shear stress on slip system n, respectively. The slip plane normal vector $v_i^{(n)}$ and slip direction vector $b_i^{(n)}$ define the Schmid tensor $P_{ij}^{(n)}$. The increment of the critical resolved shear stress is written as

$$\dot{\theta}^{(n)}=\sum_m h^{(nm)}\dot{\gamma}^{(m)}, \tag{3}$$

where $\dot{\gamma}^{(m)}$ denotes the increment of plastic shear strain on slip system m, and $h^{(nm)}$ denotes the strain-hardening coefficient.

If the slip deformation is small and rotation of the crystal orientation is neglected, the constitutive equation is written as[7]

$$\dot{\sigma}_{ij}=\left[S_{ijkl}^{e}+\sum_n\sum_m\{h^{(nm)}\}^{-1}P_{ij}^{(n)}P_{kl}^{(m)}\right]^{-1}\dot{\varepsilon}_{kl}, \tag{4}$$

where S_{ijkl}^{e} denote elastic compliance and summation is carried out over the active slip systems.

The critical resolved shear stress is assumed to be given by the following modified Bailey-Hirsch relation[8]:

$$\theta^{(n)}=\theta_0(T)+\sum_{m=1}^{12}a\mu\tilde{b}\Omega^{(nm)}\sqrt{\rho_S^{(m)}}, \tag{5}$$

where θ_0 denotes the lattice friction term, a a is numerical factor close to 0.1, μ is the elastic shear modulus, $\tilde{b}$ is the magnitude of the Burgers' vector, $\Omega^{(nm)}$ is the interaction matrix that defines the reaction between dislocations on slip systems n and m, and $\rho_S^{(m)}$ is the density of statistically stored (SS) dislocations that accumulate on slip system m. In addition, the increment of the SS dislocations is given as[8]

$$\dot{\rho}_S^{(m)}=\frac{c\dot{\gamma}^{(m)}}{\tilde{b}L^{(m)}}, \tag{6}$$

where c is a numerical coefficient on the order of 1, $L^{(n)}$ denotes the mean free path of dislocations on slip system n which is expressed by the following dislocation-density-dependent-model[9),(10)]:

$$L^{(n)}=\frac{c^*}{\sqrt{\sum_m\omega^{(nm)}\left(\rho_S^{(m)}+\left\|\rho_G^{(m)}\right\|\right)}}, \tag{7}$$

where c^* is a material constant, and $c^*=15$ is assumed in this paper. $\omega^{(nm)}$ is the dislocation interaction matrix.

The norm of the edge and screw components of the GN dislocations defines the scalar density for the GN dislocations[11]:

$$\left\|\rho_G^{(m)}\right\|=\sqrt{\left(\rho_{G,edge}^{(m)}\right)^2+\left(\rho_{G,screw}^{(m)}\right)^2}, \tag{8}$$

$$\rho_{G,edge}^{(m)}=-\frac{1}{\tilde{b}}\frac{\partial\gamma^{(m)}}{\partial\xi^{(m)}}, \quad \rho_{G,screw}^{(m)}=\frac{1}{\tilde{b}}\frac{\partial\gamma^{(m)}}{\partial\zeta^{(m)}}, \tag{9}$$

where $\xi^{(m)}$ and $\zeta^{(m)}$ denote directions parallel and perpendicular to the slip direction on the slip plane, respectively.

The strain-hardening coefficient in Eq. (3) is given by

$$h^{(nm)}=\frac{1}{2}\frac{ac\mu\Omega^{(nm)}}{L^{(m)}\sqrt{\rho_S^{(m)}}}. \tag{10}$$

3. Model

Figure 1 shows the bicrystal model employed in this study. The specimen has width $l=200$ and thickness $t=10\,\mu$m. Grain boundary planes are perpendicular to the $x-y$ planes of the model, which uniformly divide the model into 3 200 finite elements. The continuity requirements of strain components across the grain boundary plane between grains 1 and 2 are given by the following relationships[5),(6)]:

$$\varepsilon_{yy}^{(1)}=\varepsilon_{yy}^{(2)}, \quad \varepsilon_{zz}^{(1)}=\varepsilon_{zz}^{(2)}, \quad \varepsilon_{yz}^{(1)}=\varepsilon_{yz}^{(2)}, \tag{11}$$

where $\varepsilon_{yy}^{(1)}$, for example, denotes the sum of elastic and plastic strain components and the superscript denotes the grain number.

The elastic compliance data for standard crystal orientation are $S_{11}=1.0$, $S_{12}=-0.25$ and $S_{44}=2.5\,[\times10^{-11}\,\mathrm{m^2/N}]$, and the interaction of crystal grains due to the effect of the elastic incompatibility stress[11] does not occur through grain boundary planes.

Figure 2 shows the rotation crystal coordinate and Euler angles (κ, θ, ϕ). A summary of the components of the slip direction and normal direction of the slip plane on the primary slip systems is shown in Table 1. Values of the Schmid tensor for the primary slip systems are shown in Table 2, in which the initial crystal orientation of grains 1

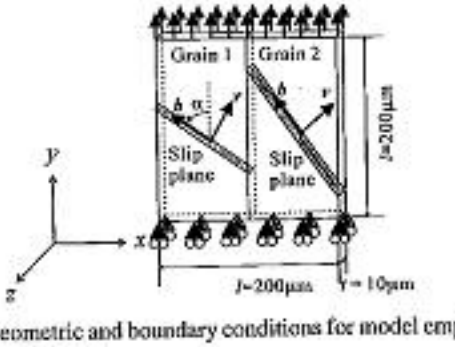

Fig. 1 Geometric and boundary conditions for model employed in this study

and 2 is selected as a combination of the same angle difference from 45° to the high- and low-angle sides. In this case, since $b_z^{(9\alpha)}$ and $b_z^{(9\alpha)}$ are equal to 0, the components of Schmid tensor, $P_{33}^{(9\alpha)}$, $P_{23}^{(9\alpha)}$ and $P_{31}^{(9\alpha)}$, are also equal to 0. Then, the increments of plastic strain $\dot{\varepsilon}_{zz}^p$, $\dot{\varepsilon}_{yz}^p$ and $\dot{\varepsilon}_{zx}^p$ are also equal to 0, Since the values of $P_{22}^{(9\alpha)}$ for grains 1 and 2 are the same, the strain $\dot{\varepsilon}_{yy}^p$ for both grains is the same and Eq. (11) is satisfied.

The initial dislocation densities ρ_0 for the twelve slip systems are assumed 1.0×10^9 [m^{-2}]. This model is deformed under tensile load in the y-axis.

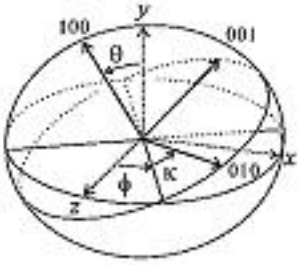

Fig. 2 Definition of Euler angles κ, θ, and ϕ

4. Analytical Results and Discussions

4.1 Effect of initial crystal orientation on GN dislocation structure

In the previous study, we observed that nonuniform deformation took place with the accumulation of high-density GN dislocations in the form of bands in symmetric bicrystal models depending on boundary conditions and the combination of the crystal orientation[5),6)], and that the GN dislocation structure exhibited nonuniform deformation behavior. In this study, we discuss the effect of asymmetric GN dislocation structure formation in bicrystal models with a tilted angle grain boundary on subsequent deformation behavior.

Figure 3 shows the difference in deformation behavior for each initial crystal orientation when the macroscopic nominal strain $\bar{\varepsilon}_{yy}$ is 0.01%. The distributions of plastic shear strain are displayed from maximum to minimum values. The edge and screw components of GN dis-

Table 1 Euler angle (κ, θ, ϕ), angle between slip direction and tensile-loading direction α, components of slip direction vector $b^{(9\alpha)}$, slip plane normal vector $n^{(9\alpha)}$, and values of Schmid tensor $P_{ij}^{(9\alpha)}$ $\left(b_z^{(9\alpha)}=b_z^{(9\alpha)}=0,\ P_{33}^{(9\alpha)}=P_{23}^{(9\alpha)}=P_{31}^{(9\alpha)}=0\right)$

Grain Num	(κ, θ, ϕ) [deg]	α [deg]	$b_x^{(9\alpha)}$	$b_y^{(9\alpha)}$	$n_x^{(9\alpha)}$	$n_y^{(9\alpha)}$	$P_{11}^{(9\alpha)}$	$P_{22}^{(9\alpha)}$	$P_{12}^{(9\alpha)}$
1	(88.414, 26.260, 67.325)	50	-0.7660	0.6428	0.6428	0.7660	-0.4924	0.4924	-0.0868
	(86.301, 25.890, 69.223)	49	-0.7547	0.6561	0.6561	0.7547	-0.4951	0.4951	-0.0696
	(84.132, 25.551, 71.177)	48	-0.7431	0.6691	0.6691	0.7431	-0.4973	0.4973	-0.0523
	(81.912, 25.245, 73.182)	47	-0.7314	0.6820	0.6820	0.7314	-0.4988	0.4988	-0.0349
	(79.645, 24.973, 75.236)	46	-0.7193	0.6947	0.6947	0.7193	-0.4997	0.4997	-0.0174
2	(74.983, 24.535, 79.469)	44	-0.6947	0.7193	0.7193	0.6947	-0.4997	0.4997	0.0174
	(72.600, 24.370, 81.639)	43	-0.6820	0.7314	0.7314	0.6820	-0.4988	0.4988	0.0349
	(70.190, 24.243, 83.835)	42	-0.6691	0.7431	0.7431	0.6691	-0.4973	0.4973	0.0523
	(67.760, 24.156, 86.052)	41	-0.6561	0.7547	0.7547	0.6561	-0.4951	0.4951	0.0696
	(65.317, 24.106, 88.282)	40	-0.6428	0.7660	0.7660	0.6428	-0.4924	0.4924	0.0868

Table 2 Slip system number, Schmid-Boas notation, and Schmid factor

Num.	Notation	Schmid factor									
		$\alpha=50$	$\alpha=49$	$\alpha=48$	$\alpha=47$	$\alpha=46$	$\alpha=44$	$\alpha=43$	$\alpha=42$	$\alpha=41$	$\alpha=40$
1	(111)[1$\bar{1}$0]	0.2507	0.2582	0.2657	0.2730	0.2803	0.2945	0.3015	0.3083	0.3151	0.3216
2	(111)[01$\bar{1}$]	0.2372	0.2269	0.2162	0.2051	0.1937	0.1699	0.1576	0.1450	0.1322	0.1191
3	(111)[10$\bar{1}$]	0.4880	0.4851	0.4818	0.4781	0.4740	0.4645	0.4591	0.4534	0.4472	0.4407
4	($\bar{1}$11)[110]	-0.2418	-0.2375	-0.2332	-0.2287	-0.2241	-0.2146	-0.2097	-0.2047	-0.1997	-0.1945
5	($\bar{1}$11)[01$\bar{1}$]	-0.0776	-0.0725	-0.0674	-0.0624	-0.0575	-0.0481	-0.0435	-0.0390	-0.0346	-0.0304
6	($\bar{1}$11)[101]	-0.1641	-0.1650	-0.1658	-0.1663	-0.1666	-0.1666	-0.1663	-0.1658	-0.1650	-0.1641
7	(11$\bar{1}$)[1$\bar{1}$0]	0.2462	0.2476	0.2486	0.2494	0.2498	0.2498	0.2494	0.2486	0.2476	0.2462
8	(11$\bar{1}$)[011]	0.2462	0.2476	0.2486	0.2494	0.2498	0.2498	0.2494	0.2486	0.2476	0.2462
9	(11$\bar{1}$)[101]	0.4924	0.4951	0.4973	0.4988	0.4997	0.4997	0.4988	0.4973	0.4951	0.4924
10	(1$\bar{1}$1)[110]	0.2552	0.2683	0.2811	0.2937	0.3060	0.3298	0.3412	0.3522	0.3630	0.3733
11	(1$\bar{1}$1)[011]	0.0866	0.0932	0.0999	0.1068	0.1137	0.1280	0.1352	0.1426	0.1500	0.1575
12	(1$\bar{1}$1)[10$\bar{1}$]	0.1686	0.1751	0.1812	0.1869	0.1923	0.2018	0.2059	0.2096	0.2129	0.2158

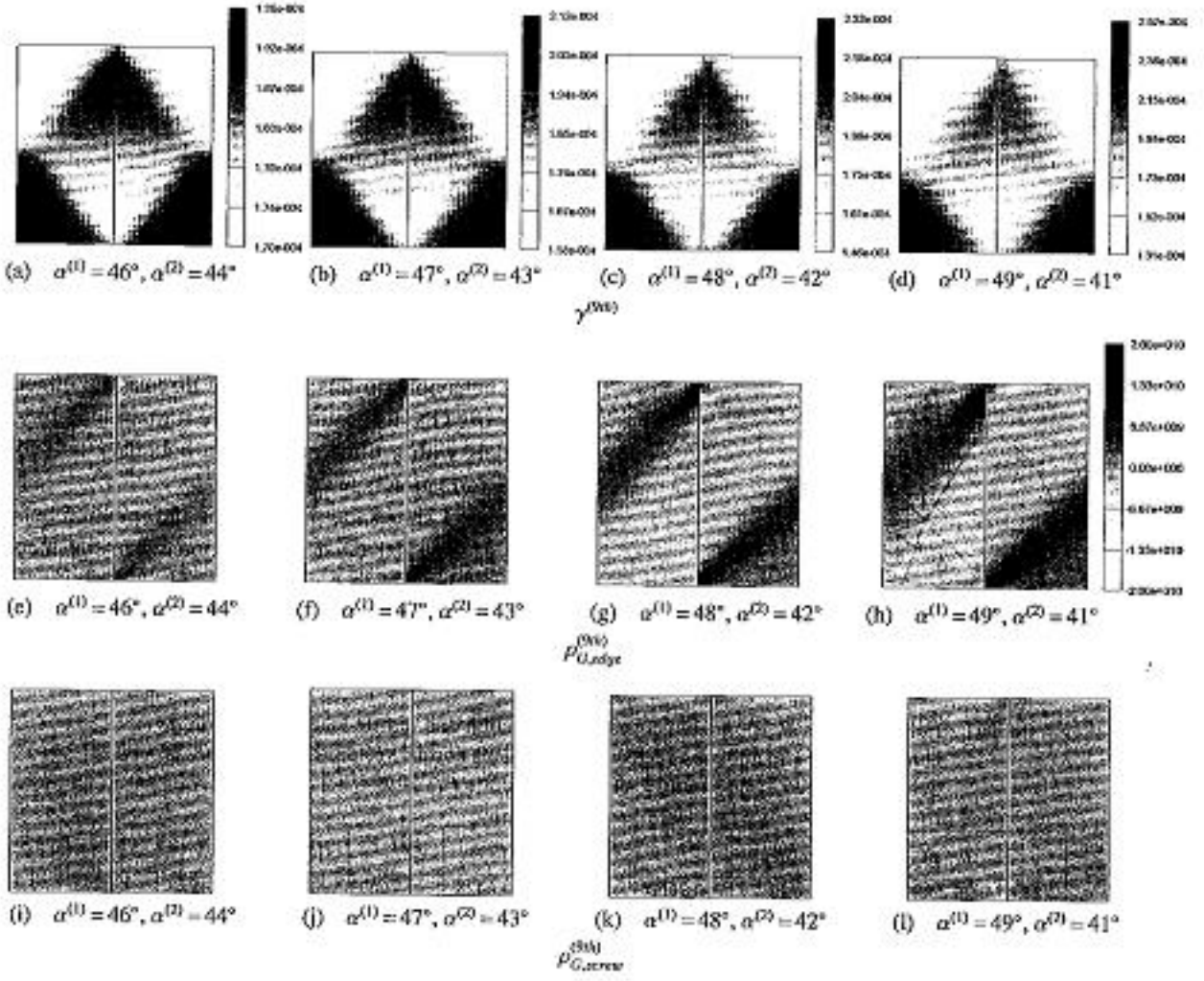

Fig. 3 (a)–(d) Distributions of plastic shear strain. Density distributions of (e)–(h) edge components and (i)–(l) screw components of GN dislocations on primary slip systems when average tensile strain $\bar{\varepsilon}_{yy}$ is 0.01%. The unit of dislocation density is m^{-2}

location density are from -2.0×10^{10} to 2.0×10^{10} [m^{-2}]. The shape change of crystal grains by free slip deformation on the primary slip system was restricted by the grain boundary and boundary condition. This is known as the incompatibility of shape change. As a result, plastic shear strain $\gamma^{(9th)}$ was distributed nonuniformly, as shown in Fig. 3 (a)–(d). Since the incompatibility of the shape change of crystal grains is asymmetric in the grain boundary, the distribution of $\gamma^{(9th)}$ becomes asymmetric in grain boundary plane. High-density GN dislocations accumulate in the form of bands from the intersection of the top (bottom) plane and the grain boundary as shown in Fig. 3 (e)–(h). This GN dislocation structure is composed of an almost perfect edge dislocation density component, in which GN dislocation density increases in proportion to the absolute value of the Schmid tensor $P_{12}^{(9th)}$ of grains 1 and 2, as shown in Fig. 3 (e)–(l).

In the result for $\alpha^{(1)}=49°$ in which GN dislocations accumulate with high density, screw dislocation density components accumulate slightly in the local area near the intersection of the top (bottom) plane and the grain boundary. This phenomenon shows the activation of secondary slip systems in the local area[6].

As shown in Table 2, for $\alpha^{(1)}>45°$, the values of the Schmid factor of the primary slip system $(111)[10\bar{1}]$ increase with the decrease in the value of Schmid factor of the secondary slip system $(1\bar{1}1)[110]$. Conversely, for $\alpha^{(1)}<45°$, the values of the Schmid factor of the primary slip system $(111)[10\bar{1}]$ decrease with the increase of the value of the Schmid factor of the secondary slip system $(1\bar{1}1)[110]$. In the case of $\alpha^{(1)}=49°$, the secondary slip system $(111)[10\bar{1}]$ becomes easily activated. Thus, the secondary slip system becomes active as an effect of the inner stress field, which is formed by the accumulation of high-density GN dislocations, on the primary slip systems, even if the macroscopic nominal strain is only 0.01%[12].

The analytical results for $\alpha^{(1)}=50°$, in which the secondary slip system $(111)[10\bar{1}]$ is more easily activated

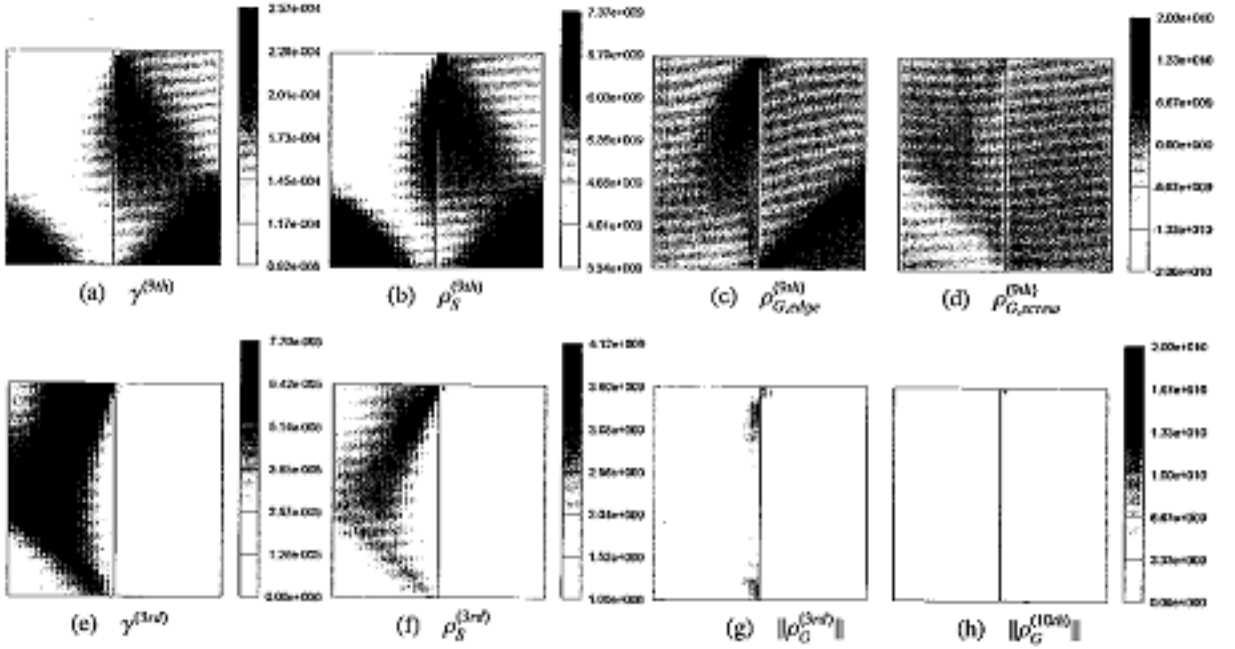

Fig. 4 (a) Distribution of plastic shear strain, (b) density distribution of statistically stored dislocations, and density distributions of (c) edge and (d) screw components of GN dislocations on primary slip systems. (e) distribution of plastic shear strain, (f) density distribution of statistically stored dislocations, and (g)–(h) density distribution of norm of GN dislocations on secondary slip systems when average tensile strain $\bar{\varepsilon}_{yy}$ is 0.1%. The unit of dislocation density is m^{-2}. $\alpha^{(1)}$ is 50°

than $\alpha^{(1)} = 45°$, are shown in Fig. 4. Since the multislip deformation of $(11\bar{1})[101]$ with $(111)[10\bar{1}]$ occurs on grain 1, as shown in Fig. 4 (a) and (e), the formation of the GN dislocations with the activation of secondary slip systems $(111)[10\bar{1}]$ becomes considerable as shown in Fig. 4 (d) and (g).

In crystal grain 2, the slip system $(1\bar{1}1)[110]$ is active in the local area near the intersection of the top (bottom) plane and the grain boundary, as shown in Fig. 4 (h). However, in other areas, the deformation behavior shows only single slip behavior on the primary slip systems $(11\bar{1})[101]$. In this way, since the spatial gradient of the plastic shear strain is induced on the primary slip system $(11\bar{1})[101]$ and the secondary slip system $(111)[10\bar{1}]$ near the grain boundary, the accumulation of GN dislocations occurs near the grain boundary area, as shown in Fig. 4 (c)–(d) and (g). Since the difference in strain-hardening between grains 1 and 2 occurs depending on the location of the active slip system, the condition of restriction interaction of deformation becomes renewed during the increase in macroscopic nominal strain.

The analytical results of macroscopic nominal strain $\bar{\varepsilon}_{yy} = 1\%$ are shown in Fig. 5. The difference between the in the distribution of SS dislocation density becomes significant depending on the difference in the active slip system between crystal grains 1 and 2, as shown in Fig. 5 (a)–(b) and (e)–(f), which indicates a considerable difference in strain hardening. In this way, deformation behavior becomes renewed during the accumulation of dislocation near grain boundaries and the subsequent formation of GN dislocations as shown in Fig. 5 (c)–(d) and (g)–(h). In particular, the renewal of the distribution of plastic shear strain on the secondary slip system $(111)[10\bar{1}]$ in crystal grain 1 is significant remarkable, as shown in Fig. 5 (e).

4.2 Estimation of pair interaction by disclination type displacement field

In the case of bicrystal models with a tilted angle grain boundary, the accumulation of GN dislocations occurs near the grain boundary, where there is a difference in active slip systems. In this case, the pair interaction of the bicrystal model becomes renewed during the increase in macroscopic nominal strain. The mechanism of the nonuniform deformation and the development of the GN dislocation structure is understood to have two stages, as shown in Fig. 6 (a)–(b) and (b)–(c). Figure 6 (a)–(b) shows the free deformation of individual crystal grains that are caused by slip on the primary slip system. Figure 6 (b)–(c) shows the interaction of crystal grains via grain boundary planes and the resulting nonuniform deformations. Mutual interaction between crystal grains and nonuniform deformation occur to satisfy boundary conditions and the continuity of the displacement through the grain boundary. The displacement field around the intersection of the top (bottom) face and the grain boundary is similar to that for wedge disclination deformation, as shown in Fig. 7 (a)–(b). In the case of twist deformation,

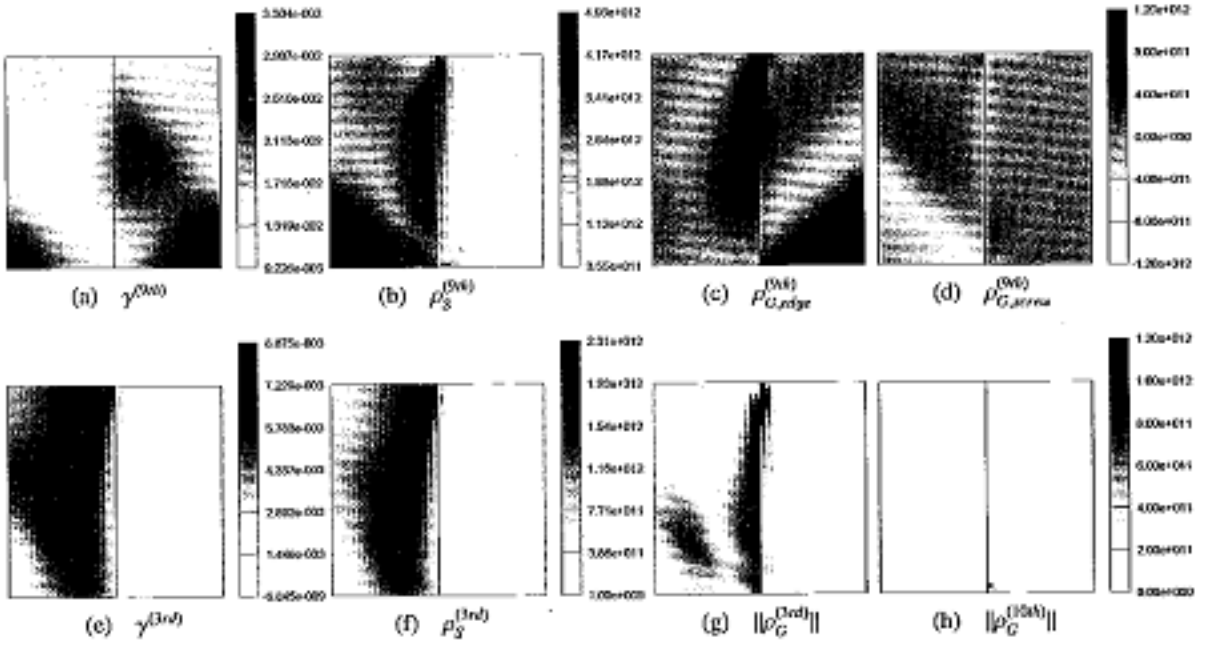

Fig. 5 (a) Distribution of plastic shear strain, (b) density distribution of statistically stored dislocations, and density distributions of (c) edge and (d) screw components of GN dislocations on primary slip systems. (e) distribution of plastic shear strain, (f) density distribution of statistically stored dislocations, (g)–(h) density distribution of norm of GN dislocations on secondary slip systems when average tensile strain $\bar{\varepsilon}_{yy}$ is 1%. The unit of dislocation density is m^{-2}. $\alpha^{(1)}$ is 50°

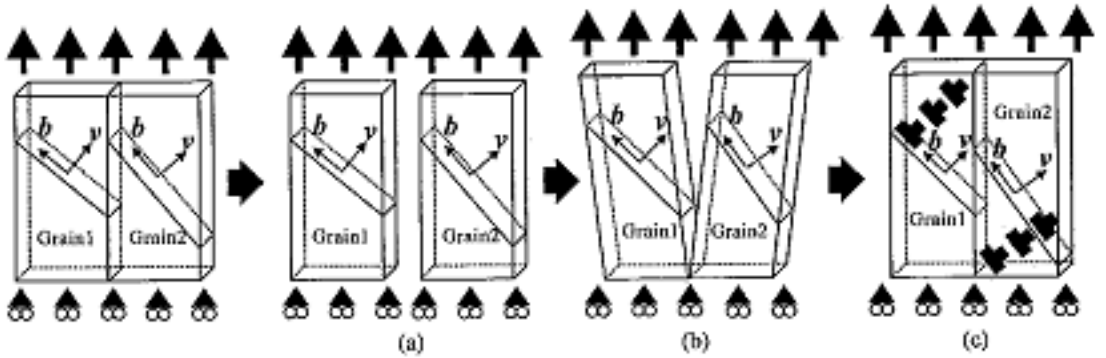

Fig. 6 Schematic illustration of (a) initial condition of compatible bicrystal with tilted angle grain boundary, (b) imaginary slip deformation without per body interaction, (c) imaginary wedge disclination deformation with per body interaction

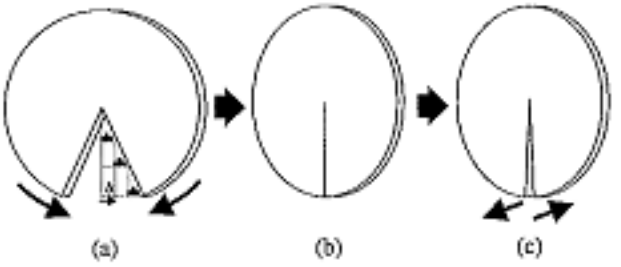

Fig. 7 Schematic illustration of (a) initial condition with dislocation, (b) wedge and (c) twist disclination deformation

the displacement field is similar to that for twist disclination deformation as shown in Fig. 7 (a)–(c) near the intersection of the top (bottom) plane and the grain boundary[13].

Wedge disclination defects spread depending on the distance from their core, and their direction is similar to the line of the edge dislocations when the direction of the disclination core is perpendicular to the direction of the Burgers vector, as shown in Fig. 7 (a). Since the line of edge dislocation is geometrically required to exist on the primary slip plane, the pattern of GN edge dislocation bands develops from intersection of the top (bottom) plane and grain boundary to inside grains 1 and 2, as shown in Fig. 3 (c)–(h).

It is well known that deformation bands (kink band and secondary slip band) indicate a stable condition of the dislocation structure, which is formed during the transient stage from stage I to stage II of slip deformation[14]. The direction of development of kink bands is perpendicular to the direction of the Burgers vector, whereas the direction of development of secondary slip bands is parallel to the primary slip plane[14]. Thus, the edge dislocation structure on primary slip systems reproduces the formation of kink bands.

Activation of the secondary slip system is necessary to develop a disclination displacement field around the intersection of the top (bottom) plane and the grain boundary during the increase in macroscopic nominal strain. The direction of the dislocation structure on the secondary slip systems in the form of bands is parallel to the primary slip plane. This formation of the GN dislocation structure on the secondary slip system results in the formation of secondary slip bands. It is possible that the superposition of the GN dislocation structure caused by the incompatibility of the shape change, and the grain boundary accumulation of GN dislocations caused by strain incompatibility will be estimated from the considering the twist disclination displacement field, as shown in Fig. 5 (c) – (d).

In this way, the asymmetric nonuniform deformation and formation of the GN dislocation structure in the bicrystal models with a tilted angle grain boundary are related to and estimated by the imaginary disclination displacement field around the intersection of the top (bottom) plane and the grain boundary.

5. Conclusion

The effects of asymmetric nonuniform deformations with the formation of a GN dislocation structure on the subsequent deformation behavior were studied in detail. The results are as follows.

(1) The grain boundary accumulation of GN dislocations was caused by the difference in strain hardening on the active slip system, and the formation of the GN dislocation structure was caused by the incompatibility of shape change induced by slip deformation in the compatible bicrystal model with a tilted angle grain boundary.

(2) Nonuniform deformation and formation of the GN dislocation structure in the bicrystal model were related to and estimated by the imaginary disclination displacement field around the intersection of the top (bottom) plane and the grain boundary.

(3) The defect of the imaginary disclination displacement field can be shown as the line of an edge dislocation, which is geometrically necessary on the primary slip system. As a result, the shape-change incompatibility was composed of a single slip of a primary slip system, whereas the GN dislocation structure was composed of an edge dislocation component in the form of bands from the imaginary disclination core perpendicular to the slip direction. This formation of the GN edge dislocation structures on the primary slip system reproduced the formation of kink bands.

(4) Activation of the secondary slip system was necessary to develop a disclination displacement field around the intersection of the top (bottom) plane and the grain boundary during the increase in macroscopic nominal strain. In addition, the direction of the dislocation structure on the secondary slip system in the form of bands is parallel to the primary slip plane. This formation of the GN dislocation structure on the secondary slip system resulted in the formation of secondary slip bands.

References

(1) Hook, R.E. and Hirth, J.P., The Deformation Behavior of Isoaxial Bicrystals of Fe-3% Si, Acta Metall., Vol.15 (1967), pp.535–551.

(2) Ashby, M.F., The Deformation of Plastically Non-Homogeneous Alloys, Phil. Mag., Vol.21 (1970), pp.399–424.

(3) Livingston, J.D. and Chalmers, B., Multi Slip in Bicrystal Deformation, Acta Metall., Vol.5, No.6 (1957), pp.322–327.

(4) Hauser, J.J. and Chalmers, B., The Plastic Deformation of Bicrystals of F.C.C. Metals, Acta Metall., Vol.9, No.9 (1961), pp.802–818.

(5) Kondou, R. and Ohashi, T., Crystal Plasticity Analysis of Non-Uniform Deformation in Symmetric Type Bi-Crystals under Tensile Load and Formation of Geometrically Necessary Dislocation Bands, Trans. Jpn. Soc. Mech. Eng., (in Japanese), Vol.71, No.705, A (2005), pp.809–816.

(6) Kondou, R. and Ohashi, T., Relationship between Formation of Geometrically Necessary Dislocations and Local Strain Hardening of Slip Systems in Symmetric Type Bi-Crystals under Tensile Loading, Trans. Jpn. Soc. Mech. Eng., (in Japanese), Vol.71, No.711, A (2005), pp.1451–1458.

(7) Hill, R., Generalized Constitutive Relations for Incremental Deformation of Metal Crystals by Multislip, J. Mech. Phys. Sol., Vol.14 (1966), pp.95–102.

(8) Ohashi, T., Numerical Modeling of Plastic Multislip in Metal Crystals of F.C.C. Type, Phil. Mag. A, Vol.70, No.5 (1994), pp.793–803.

(9) Ohashi, T., A New Model of Scale Dependent Crystal Plasticity Analysis, IUTAM Symposium on Mesoscopic Dynamics of Fracture Process and Materials Strength, (2004), pp.97–106.

(10) Ohashi, T., Prediction of Macroscopic Mechanical Response of Metallic Materials through Evaluation of Deformation Processes in Microstructure, The Iron and Steel Institute of Japan, 180-181 Nishiyama Anniversary Technique Lecture, (in Japanese), (2004), pp.73–95.

(11) Ohashi, T., Finite-Element Analysis of Plastic Slip and Evolution of Geometrically Necessary Dislocations in F.C.C. Crystals, Phil. Mag. Lett., Vol.75, No.2 (1997), pp.51–57.

(12) Ohashi, T., Meso-Scale Perspectives in the Analysis of Crystal Slip Deformation and Dislocation Accumulation, Trans. Jpn. Soc. Mech. Eng., (in Japanese), Vol.68, No.675, A (2002), pp.1490–1497.
(13) Kato, M., Dislocation Theory, (in Japanese), (1999), p.168, Shokabo.
(14) Higashida, K., Takamura, J. and Narita, N., The Formation of Deformation Bands in F.C.C. Crystals, Mat. Sci. Eng., Vol.81 (1986), pp.239–258.